Published in final edited form as:
Semin Musculoskelet Radiol. 2010 June ; 14(2): . doi:10.1055/s-0030-1253167.

Biochemical and Physiological MR Imaging of Skeletal Muscle at 7 Tesla and Above

Gregory Chang, M.D.[1], **Ligong Wang, Ph.D.**[1], **Arturo Cárdenas-Blanco, Ph.D.**[2,3,4], **Mark E. Schweitzer, M.D.**[5], **Michael P. Recht, M.D.**[1], and **Ravinder R. Regatte, Ph.D.**[1]

[1]Department of Radiology, Center for Biomedical Imaging, New York University School of Medicine, New York, New York

[2]Department of Radiology, Ottawa Hospital Research Institute, Ottawa, Ontario, Canada

[3]Department of Orthopedic Surgery, Ottawa Hospital Research Institute, Ottawa, Ontario, Canada

[4]Department of Neuroscience, Ottawa Hospital Research Institute, Ottawa, Ontario, Canada

[5]Department of Diagnostic Imaging, Ottawa General Hospital, Ottawa, Ontario, Canada

Abstract

Ultra-high field (UHF; ≥7 T) magnetic resonance imaging (MRI), with its greater signal-to-noise ratio, offers the potential for increased spatial resolution, faster scanning, and, above all, improved biochemical and physiological imaging of skeletal muscle. The increased spectral resolution and greater sensitivity to low-gamma nuclei available at UHF should allow techniques such as ^{1}H MR spectroscopy (MRS), ^{31}P MRS, and ^{23}Na MRI to be more easily implemented. Numerous technical challenges exist in the performance of UHF MRI, including changes in relaxation values, increased chemical shift and susceptibility artifact, radiofrequency (RF) coil design/B_1^+ field inhomogeneity, and greater RF energy deposition. Nevertheless, the possibility of improved functional and metabolic imaging at UHF will likely drive research efforts in the near future to overcome these challenges and allow studies of human skeletal muscle physiology and pathophysiology to be possible at ≥7 T.

Keywords

Ultra high field; MRI; muscle; spectroscopy; ultra short echo time; T_2 mapping; sodium

Skeletal muscle is the largest organ in the human body and functions to generate force and produce movement. Basically, a muscle acts to move one skeletal structure in reference to a distal structure transmitting this force via a tendon. Its tissue architecture is highly hierarchically organized, with each muscle divided by connective tissue into bundles (fascicles) of muscle fibers, which themselves represent multinucleated cells composed of myofibrils. The connective tissue that divides skeletal muscle into fascicles and fibers, perimysium and endomysium, contains a rich network of blood vessels and capillaries that transport oxygen and nutrients to muscle fibers and maintain homeostasis for the extracellular environment by carrying away heat, waste products, and electrolytes that accumulate during muscle activation.

Address for correspondence and reprint requests: Gregory Chang, M.D., Department of Radiology, Center for Biomedical Imaging, New York University School of Medicine, 660 First Ave., New York, NY 10016 (gregory.chang@nyumc.org).

Magnetic resonance imaging (MRI) has been a powerful noninvasive technique for biomedical scientists and physicians to evaluate skeletal muscle structure and function in vivo, allowing insight into muscle physiology and pathophysiology. Beyond the evaluation of anatomical features of muscle using conventional MR techniques, numerous biochemical and physiological properties of muscle have been studied including muscle fiber activation via ^{1}H MR T_2 mapping; muscle oxygenation via blood oxygenation level-dependent (BOLD) techniques; muscle perfusion via arterial spin labeling and dynamic contrast-enhanced techniques; and muscle metabolism via ^{1}H, ^{13}C, ^{31}P MR spectroscopy (MRS), and ^{23}Na MRI.[1–4]

Ultra-high field (UHF, ≥7 T) MRI, with its greater signal-to-noise ratio (SNR), has the potential to improve on our ability to evaluate the musculoskeletal system by enabling higher spatial resolution imaging and faster scanning.[5,6] More importantly, UHF MRI facilitates the performance of techniques that are SNR limited in vivo at standard clinical field strength, such as imaging of low-gamma nuclei. To reach the potential of UHF MRI, numerous technical obstacles must be surmounted, including increased chemical shift and susceptibility artifact, changes in T_1 and T_2 relaxation values, radiofrequency (RF) coil design, B_1 field inhomogeneity, and greater RF energy deposition.

This article provides a brief overview of the technical considerations for UHF MRI of the musculoskeletal system and then reviews the current status of biochemical and physiological MR techniques for evaluating skeletal muscle at 7 T.

TECHNICAL CONSIDERATIONS OF ULTRA HIGH FIELD MRI

The motivation for the development of UHF MR systems stems from the increased intrinsic SNR available at higher magnetic fields. In general, in an MR experiment, the signal from a sample is proportional to the square of the static magnetic field (B_0^2). Noise, in contrast, results from noise from the coil and noise from the imaging sample. By treating the coil and the sample as resistors in series and by modeling the power dissipated in the coil and the power dissipated in the sample based on principles of conductivity in a wire and Faraday's law, SNR can be given by this equation:

$$\frac{Signal}{Noise} \sim \frac{B_0^2}{Noise_{coil} + Noise_{sample}} = \frac{B_0^2}{\sqrt{aB_0^{1/2} + bB_0^2}}$$

where the terms $aB_0^{1/2}$ and bB_0^2 represent the contributions from coil noise and sample noise, respectively.[7,8] With increasing field strength, the sample noise predominates over the coil noise, and as a result, SNR scales approximately linearly with B_0. (In actuality, the situation is more complicated than this, and a thorough treatment of SNR at UHF is given in Collins[8]).

As stated earlier, the increased SNR of UHF can be translated into greater spatial and/or temporal resolution, the ability to do nonproton imaging, and significant improvements in functional imaging. However, there are technical challenges that must be surmounted before the full potential of UHF MR can be reached. These technical challenges are discussed next.

In general, for ^{1}H MRI, T_1 values increase[9] and T_2 values decrease with increasing field strength.[10,11] T2* relaxation times disproportionately decrease secondary to greater macroscopic and microscopic susceptibility effects in the larger static field.[10,11] These changes in T_1 and T_2 relaxation times require sequence parameters to be adjusted when imaging at UHF compared with standard clinical field strength.

Increased chemical shift artifact must also be taken into consideration when imaging at UHF.[5] For example, the chemical shift difference between water and fat resonance at 7 T is ~1040 Hz compared with ~440 Hz at 3 T and ~220 Hz at 1.5 T. At a bandwidth of 130 Hz, this corresponds to a chemical shift of 8 pixels at 7 T, versus 3.4 pixels at 3 T and 1.7 pixels at 1.5 T. Increased chemical shift artifact will result in greater pixel misregistration on images. However, it should be noted that the greater frequency separation between fat and water at increasing field strength translates into improved spectral resolution for MRS studies performed at UHF.

The performance of UHF MRI also presents challenges for RF coil design. Quasistatic field approximations that have been used for circuit modeling of lower field RF coils can no longer accurately describe the interactions of electromagnetic waves with the human body, and full-wave methods are required.[12–15] RF coils must be designed to limit signal losses to the coil circuit, magnet bore environment, and tissue of interest, in addition to being designed to control RF field propagation and minimize energy deposition.

Related to the challenge of RF coil design is the challenge of greater variation in the B_1^+ field at 7 T. At 7 T, the Larmor frequency of protons is 300 MHz, which means that the wavelengths of electromagnetic waves become on the order of the size of the human head/body.[10] Depending on its local dielectric properties, the tissue of interest can act as a radiofrequency resonator, and as a result, the RF coil no longer solely defines the RF field.[11] Standing waves can be created that result in constructive and destructive interference patterns that will increase and decrease B_1 field strength, respectively. These effects are less important in the extremities (because of the smaller dimensions compared with the head and body), but they may become pertinent when imaging the pelvis or paraspinal and abdominal musculature. RF shimming and transmission arrays will certainly contribute to improvements in image quality and maintenance of B_1^+ homogeneity at UHF.

A final challenge for UHF MRI is increased RF energy deposition in tissue, which can result in heating. Current Food and Drug Administration (FDA) and Center for Devices and Radiologic Health (CDRH) limits for specific absorption rate are 4 W/kg averaged over a 15-minute period for the whole-body and 12 W/kg averaged over 5 minutes in any 1 g of tissue in the extremities. In theory, energy deposition will vary with the square of the Larmor frequency (ω_0), which itself scales linearly with B_0. However, there is evidence suggesting that beyond 250 MHz, the ω_0^2 rule does not hold true, and energy deposition may be linearly related to B_0.[13,16,17] This would be advantageous for UHF MR because SNR improvement could be maintained while preserving patient safety. Improvements in multichannel coil techniques and pulse sequence modifications developed for 3 T are the best strategies to ameliorate these difficulties at ≥7 T.

ANATOMICAL IMAGES OF MUSCLE

Despite alterations in T1 and T2 relaxation times with increasing field strength, the appearance of muscle on 7-T images is similar to that obtained at standard clinical field strength.

Figs. 1A and B show axial T1- and T2-weighted images of muscles of the human thigh obtained from different subjects at 7 T with an in-plane spatial resolution ranging from 0.253 mm to 0.625 mm, and with a slice thickness of 1 to 2 mm. There is flow-related enhancement within the arteries on T1-weighted images, which were obtained with a gradient-recalled echo sequence.

Figs. 2A and B show axial T1- and T2-weighted images of the human calf obtained from different subjects at 7 T with an in-plane spatial resolution ranging from 0.292 mm to 0.585

mm, and with a slice thickness of 2 mm. On T2-weighted images, there is pulsation artifact and coil inhomogeneity artifact near the periphery of the field of view (FOV).

Figs. 3A and B show axial high-resolution 11.7-T MR images of the tibiae and fibulae from male Sprague-Dawley rats obtained ex vivo. Fig. 3A was obtained with a gradient-echo sequence (TR/TE, 500/5.07) and an in-plane spatial resolution of 66 microns (FOV, 1.7 cm × 1.7 cm; matrix, 256 × 256) and a slice thickness of 0.5 mm. Fig. 3B was obtained with a spin-echo sequence (TR/TE, 2500/8.07) and an in-plane spatial resolution of 33 microns (FOV, 1.6 cm × 1.6 cm; matrix, 512 × 512) and a slice thickness of 0.5 mm. As expected, there is chemical shift artifact in Fig. 3A, the gradient-echo image. The diameter of the bore for the 11.7-T MR scanner is 8.9 cm and thus is only suitable for small animal studies.

^{1}H MR SPECTROSCOPY

^{1}H MR spectroscopy has been used successfully for many clinical and research applications in skeletal muscle including evaluation of: intramyocellular lipids (IMCL, reviewed extensively in Boesch et al[3] and Boesch[4]); lactate formation in subjects before and after exercise;[18–21] total creatine content;[22] tissue oxygenation/deoxygenation[23] (also reviewed extensively in Carlier et al[2]); and metabolite diffusion.[24]

At 7 T, preliminary studies have focused on the evaluation of IMCL, which at standard clinical field strength has been shown to be elevated in subjects with type 2 diabetes and insulin resistance, and in well-trained athletes with high insulin sensitivity.[4] IMCL has also been shown to be depleted during strenuous exercise.[25–27] In theory, MRS of skeletal muscle in vivo should be improved at UHF secondary to the greater signal available and greater spectral resolution/increased frequency separation between metabolites.

Wang et al performed single voxel MRS of the tibialis anterior muscle in human subjects in vivo and measured T1 and T2 relaxation times of skeletal muscle metabolites.[28] They found that at 7 T, there is an increase in T1 relaxation times and decrease in T2 relaxation times of skeletal muscle metabolites compared with 3 T (Table 1). Furthermore, at 7 T, the lipid spectra are better resolved compared with 3 T, with multiple peaks that are measurable at 7 T but not visible at 3 T (Fig. 4).

Khuu et al used an approach called fiber orientation modeling (FOM) to determine the effect of the orientation of extracellular fat on simulated and in vivo lipid spectra from healthy human subjects at 7 T.[29] They found that the estimated IMCL concentration in the gastrocnemius and soleus was significantly lower when the extramyocellular lipid (EMCL) signal was assumed to originate from multiple strands of fat with variable orientations relative to B_0. The results of this work will allow more accurate quantitation of IMCL to be performed at UHF in the future.

Versluis et al used a new technique called volume-selective power optimization at 7 T to calibrate RF pulses for spectroscopic studies of human calf muscles.[30] Compared with conventional power calibration techniques, increases in SNRs based on unsuppressed water signal in the calf of healthy human volunteers was between 22 ± 5% and 166 ± 42%. Such a technique will help realize the full SNR potential of UHF MRI.

And finally, Fissoune et al demonstrated the feasibility of performing ^{1}H MRS on mouse skeletal muscle to assess IMCL at 7 T.[31] They found that IMCL in the tibialis anterior muscle of diabetic mice was increased relative to control littermates and that older mice have greater IMCL levels than younger mice.

Altogether, the improved spectral resolution and sensitivity of UHF MR holds promise for MRS studies of skeletal muscle. The spectra obtained at 7 T reveal that what were previously considered single peaks at 1.5 T and even 3 T, actually represent the coalescence of several metabolites. Protocol optimization and feasibility studies will be important in the near future before UHF techniques can be applied to subjects with disease.

^{1}H MR T_2 MAPPING

An increase in signal intensity in skeletal muscle on T2-weighted images following exercise was first described by Fleckenstein et al in 1988.[32] This phenomenon has been attributed to the exercise-induced accumulation of intra-cellular osmolites and metabolites and subsequent shift of water from the extracellular to intracellular space, which together cause an increase in T2 relaxation values for skeletal muscle.[33–36]

At New York University (NYU), we have performed preliminary studies in a limited number of subjects (unpublished data) evaluating skeletal muscle T2 relaxation values before and after exercise at 7 T. Using a multiple-echo-spin-echo sequence and a mono-exponential best-fit model, resting T2 values for muscles of the calf in humans have been calculated to be 33.9 ± 3.78 ms, 36.8 ± 4.2 ms, 36.7 ± 4.67 ms, for tibialis anterior, soleus, and gastrocnemius, respectively. After plantar flexion exercise these values increased ~12 to 17%, then decreased to baseline in a logarithmic fashion with a half-life of 12 to 15 minutes. Overall, the calculated T2 values for skeletal muscle and the time course of recovery for T2 values after exercise are similar to those described at lower field strength. To our best knowledge, T2 mapping of muscle has not previously been reported at UHF.

Although it is feasible to perform skeletal muscle T2 mapping at UHF, the benefit beyond performing these studies at 1.5 T or 3 T remains to be determined. One possible benefit might lie in the higher spatial resolution imaging that is possible at 7 T. Higher spatial resolution images might allow subregions or motor units within a muscle to be identified. A method to identify subregional muscle activity would improve on clinicians' and researchers' ability to identify pathological muscle fibers in aging and neuromuscular disorders, and it would allow more refined analyses of treatment response to exercise and rehabilitation interventions. However, before such studies can be performed, much work remains, including the optimization of sequence parameters and the determination of how perfusion and oxygenation (in particular, BOLD-related T2 shortening effects) might affect T2 mapping at 7 T.

^{1}H-ULTRASHORT ECHO-TIME MR

Using conventional MR imaging techniques, musculoskeletal tissues with extremely fast transverse relaxation (tendons, cortical bone) normally demonstrate little to no signal on T2-weighted images. Ultra-short echo-time (UTE) MRI provides a method to evaluate these tissues before their signal has decayed. This has been successfully applied as a method to evaluate cortical bone porosity/water content as a marker of bone strength[37,38] and as a method to evaluate the biochemical content of tendons, which may undergo changes in their molecular composition before they begin to tear on a macroscopic level.[39,40]

Fig. 5A and B show 7-T MR images of the thigh obtained at NYU with a three-dimensional (3D) radial acquisition water excitation sequence (TR, 250 ms; 25,000 projections, 1.48 mm × 1.48 mm × 1.48 mm) with echo times of 0.300 ms and 4.4 ms, respectively. The 3D radial sequence is well suited for short TE imaging because no slice selection pulse is required, thus minimizing the delay between excitation and data acquisition. In addition, the k-space trajectory begins at the origin of k-space, allowing efficient sampling of low-frequency, high-amplitude data. On the UTE image (Fig. 5A; TE, 0.300), the quadriceps tendon is

uniformly hyperintense in signal. On the longer TE image (Fig. 5B; TE, 4.4), there is only minimal hyperintensity within the central portion of the quadriceps tendon. Images such as these might be used in the future to evaluate tendon degeneration at 7 T.

^{23}Na Magnetic Resonance Imaging

Sodium ions play a critical role in muscle and cellular physiology. The concentration gradient of sodium across the cell membrane (140 mmol in the extracellular space, 10 to 15 mmol/L in the intracellular space) contributes to the resting membrane potential, which provides stored energy for processes such as membrane transport and allows the generation of action potentials leading to muscle contraction.

Sodium has a 3/2 spin nucleus and an electric quadripolar moment that distorts the nonsymmetrical spherical distribution of charge around the nucleus.[41] In biological tissues in vivo, the sodium signal is ~1/20,000 that of protons. Detection of the sodium MR signal is further hindered by its low gyromagnetic ratio (11.3 MHz/T) and its fast T2 relaxation time, which in the intermediate regime of biological tissues is biexponential with a short component of ~0.5 to 8 ms, and a longer component of ~15 to 30 ms.

At 1.5 T and 3 T, ^{23}Na MRI has been used to evaluate skeletal muscle in healthy subjects after exercise,[42,43] in subjects with paramyotonia congenita,[44,45] and in subjects with myotonic dystrophy.[42] In these studies, increased sodium signal intensity was seen in stimulated muscles used during exercise and in the muscles of people affected by paramyotonia congenita or myotonic dystrophy.

At NYU, we have performed preliminary ^{23}Na MR studies of skeletal muscle at 7 T in healthy volunteers using a sodium volume coil and by implementing a 3D-radial acquisition sequence with a UTE of 160 μs (unpublished data). Improved imaging is enabled not only by the increased signal available at 7 T, but also by the use of the UTE sequence, which minimizes T2 signal loss, and the radial acquisition, which allows sampling of data without the need for a slice selection pulse.

Representative images of resting skeletal muscle of the calf are shown in Fig. 6A. There is uniform signal intensity in resting muscles. After 3 minutes of plantar flexion exercise, there is an increase in muscle signal intensity within the posterior compartment muscles used in the exercise, gastrocnemius, and soleus, but no increase in signal intensity in tibialis anterior, an extensor compartment muscle not used in the exercise (Fig. 6B). In the future, such studies might provide insight into electrolyte balance and muscle physiology during exercise.

^{31}P MR SPECTROSCOPY

^{31}P MR spectroscopy can provide insight into skeletal muscle bioenergetics. Previous studies have used ^{31}P MRS techniques to determine oxidative capacity in well-trained athletes, who have been shown to have higher phosphocreatine/inorganic phosphate (PCr/Pi) ratios for a given workload,[46–48] and faster recovery of PCr after exercise.[47,49] It has also been used as a tool to study McArdle's disease,[50–53] glycogen storage disease type XIII,[54] phosphofructokinase deficiency,[55,56] mitochondrial diseases,[57–59] peripheral arterial disease,[60,61] type 2 diabetes,[62] and aging.[63–65]

Bogner et al measured T1 and T2 relaxation times of ^{31}P metabolites in resting human skeletal muscle at 3 T and 7 T.[66] They found a statistically significant decrease in T1 relaxation values for phosphomonoesters, phosphodiesters, PCr, and various nucleotide triphosphates (NTPs) but not for Pi. They also found a statistically significant decrease in T2

relaxation values for Pi, phosphodiesters, phosphocreatine, and γ-NTP. The decrease in T_1 values at 7 T was attributed to the increasing influence of chemical shift anisotropy on relaxation mechanisms at higher field strength. They also found that twice as much SNR was offered at 7 T compared with 3 T and that higher quality spectra were generated as demonstrated by broader line widths. The intrinsically higher SNR, in combination with shorter T1 values, meant that per unit acquisition time, the SNR increase at 7 T was actually 150% compared with 3 T under their scanning conditions.

OTHER TECHNIQUES

Numerous other MR techniques to evaluate skeletal muscle physiology have been described, including evaluation of muscle perfusion via arterial spin labeling and dynamic contrast enhancement; evaluation of muscle oxygenation via BOLD techniques; evaluation of muscle architecture and biomechanical properties via diffusion tractography and MR elastography; evaluation of carbohydrate metabolism via ^{13}C MR spectroscopy; and evaluation of the phosphocreatine-creatine system via magnetization transfer techniques.[1,2] Magnetization transfer has been applied to assess the transfer of magnetization between the free metabolite pool (phosphocreatine/creatine) and the motion-restricted proton pool, and it shows promise as an adjunct to other metabolic muscle imaging techniques.[1]

Although many of these techniques have been performed in the brain at UHF, to our best knowledge, they have not yet been performed at UHF in the musculoskeletal system. Performance of ^{13}C MRS in muscle could certainly benefit from the increased SNR and spectral resolution at 7 T. Arterial spin labeling, which is technically challenging at 1.5 T due to low SNR and the short T1 relaxation value of blood, will also likely benefit from the transition to UHF because SNR will be greater and T1 relaxation values will be increased, allowing easier detection of signal differences between labeled and unlabeled inflowing blood signal images.[11] Finally, there is strong evidence that BOLD MR techniques in the brain demonstrate increased sensitivity, specificity, and spatial accuracy at UHF,[67,68] and this will likely hold true when these techniques are used in the musculoskeletal system in the future.

CONCLUSION

MR imaging of the musculoskeletal system at UHF strength is at its inception. The proliferation of UHF systems at numerous academic centers around the world will help pave the way for the development of biochemical and functional musculoskeletal MR techniques as powerful noninvasive methods to gain insight into muscle physiology and pathophysiology, potentially allowing earlier diagnosis of disease and more accurate monitoring of disease progression.

Acknowledgments

The authors would like to acknowledge support from the RSNA (RR0806) and NIAMS/NIH (R01-AR053133-01A2).

References

1. Prompers JJ, Jeneson JA, Drost MR, Oomens CC, Strijkers GJ, Nicolay K. Dynamic MRS and MRI of skeletal muscle function and biomechanics. NMR Biomed. 2006; 19(7):927–953. [PubMed: 17075956]
2. Carlier PG, Bertoldi D, Baligand C, Wary C, Fromes Y. Muscle blood flow and oxygenation measured by NMR imaging and spectroscopy. NMR Biomed. 2006; 19(7):954–967. [PubMed: 17075963]

3. Boesch C, Machann J, Vermathen P, Schick F. Role of proton MR for the study of muscle lipid metabolism. NMR Biomed. 2006; 19(7):968–988. [PubMed: 17075965]
4. Boesch C. Musculoskeletal spectroscopy. J Magn Reson Imaging. 2007; 25(2):321–338. [PubMed: 17260389]
5. Regatte RR, Schweitzer ME. Ultra-high-field MRI of the musculoskeletal system at 7. 0T. J Magn Reson Imaging. 2007; 25(2):262–269. [PubMed: 17260399]
6. Krug R, Stehling C, Kelley DA, Majumdar S, Link TM. Imaging of the musculoskeletal system in vivo using ultra-high field magnetic resonance at 7 T. Invest Radiol. 2009; 44(9):613–618. [PubMed: 19652609]
7. Hoult DI, Lauterbur PC. The sensitivity of the zeugmato-graphic experiment involving human samples. J Magn Reson. 1979; 34:425–433.
8. Collins, CM. Radiofrequency field calculations for high field MRI. In: Robitaille, PM.; Berliner, LJ., editors. Ultra High Field Magnetic Resonance Imaging. New York, NY: Springer; 2006. p. 209-248.
9. Bottomley PA, Foster TH, Argersinger RE, Pfeifer LM. A review of normal tissue hydrogen NMR relaxation times and relaxation mechanisms from 1–100 MHz: dependence on tissue type, NMR frequency, temperature, species, excision, and age. Med Phys. 1984; 11(4):425–448. [PubMed: 6482839]
10. Pruessmann KP. Parallel imaging at high field strength: synergies and joint potential. Top Magn Reson Imaging. 2004; 15(4):237–244. [PubMed: 15548954]
11. Schmitt, F.; Potthast, A.; Stoeckel, B., et al. Aspect of clinical imaging at 7T. In: Robitaille, PM.; Berliner, LJ., editors. Ultra High Field Magnetic Resonance Imaging. New York, NY: Springer; 2006. p. 59-103.
12. Ibrahim TS, Lee R, Baertlein BA, Kangarlu A, Robitaille PL. Application of finite difference time domain method for the design of birdcage RF head coils using multi-port excitations. Magn Reson Imaging. 2000; 18(6):733–742. [PubMed: 10930783]
13. Vaughan JT, Garwood M, Collins CM, et al. 7T vs. 4T: RF power, homogeneity, and signal-to-noise comparison in head images. Magn Reson Med. 2001; 46(1):24–30. [PubMed: 11443707]
14. Wei Q, Liu F, Xia L, Crozier S. An object-oriented designed finite-difference time-domain simulator for electromagnetic analysis and design in MRI—applications to high field analyses. J Magn Reson. 2005; 172:222–230. [PubMed: 15649749]
15. Beck BL, Jenkins K, Caserta J, Padgett K, Fitzsimmons J, Blackband SJ. Observation of significant signal voids in images of large biological samples at 11. 1 T. Magn Reson Med. 2004; 51(6):1103–1107. [PubMed: 15170828]
16. Collins CM, Smith MB. Signal-to-noise ratio and absorbed power as functions of main magnetic field strength, and definition of “90 degrees” RF pulse for the head in the birdcage coil. Magn Reson Med. 2001; 45(4):684–691. [PubMed: 11283997]
17. Ibrahim TS. A numerical analysis of radiofrequency power requirements in magnetic resonance imaging experiments. IEEE Trans Microw Theory Tech. 2004; 52(8):1999–2003.
18. Hetherington HP, Hamm JR, Pan JW, Rothman DL, Shulman RG. A fully localized 1H homonuclear editing sequence to observe lactate in human skeletal muscle after exercise. J Magn Reson. 1989; 82:86–96.
19. Pan JW, Hamm JR, Hetherington HP, Rothman DL, Shulman RG. Correlation of lactate and pH in human skeletal muscle after exercise by 1H NMR. Magn Reson Med. 1991; 20(1):57–65. [PubMed: 1943662]
20. Jouvensal L, Carlier PG, Bloch G. Practical implementation of single-voxel double-quantum editing on a whole-body NMR spectrometer: localized monitoring of lactate in the human leg during and after exercise. Magn Reson Med. 1996; 36(3):487–490. [PubMed: 8875423]
21. Brillault-Salvat C, Giacomini E, Wary C, et al. An interleaved heteronuclear NMRI-NMRS approach to non-invasive investigation of exercising human skeletal muscle. Cell Mol Biol (Noisy-le-grand). 1997; 43(5):751–762. [PubMed: 9298597]
22. Brault JJ, Towse TF, Slade JM, Meyer RA. Parallel increases in phosphocreatine and total creatine in human vastus lateralis muscle during creatine supplementation. Int J Sport Nutr Exerc Metab. 2007; 17(6):624–634. [PubMed: 18156666]

23. Wang ZY, Noyszewski EA, Leigh JS Jr. In vivo MRS measurement of deoxymyoglobin in human forearms. Magn Reson Med. 1990; 14(3):562–567. [PubMed: 2355838]
24. Kruiskamp MJ, De Vilder SJ, De Graaf RA, Nicolay K. 31P/ and 1H/MRS measurements of metabolite diffusion in rat and mouse hindleg skeletal muscle. Proc ISMRM. 1999; 7:697.
25. Decombaz J, Schmitt B, Ith M, et al. Postexercise fat intake repletes intramyocellular lipids but no faster in trained than in sedentary subjects. Am J Physiol Regul Integr Comp Physiol. 2001; 281:R760–R769. [PubMed: 11506990]
26. Thamer C, Machann J, Bachmann O, et al. Intramyocellular lipids: anthropometric determinants and relationships with maximal aerobic capacity and insulin sensitivity. J Clin Endocrinol Metab. 2003; 88(4):1785–1791. [PubMed: 12679474]
27. Goodpaster BH, He J, Watkins S, Kelley DE. Skeletal muscle lipid content and insulin resistance: evidence for a paradox in endurance-trained athletes. J Clin Endocrinol Metab. 2001; 86(12): 5755–5761. [PubMed: 11739435]
28. Wang L, Salibi N, Wu Y, Schweitzer ME, Regatte RR. Relaxation times of skeletal muscle metabolites at 7T. J Magn Reson Imaging. 2009; 29(6):1457–1464. [PubMed: 19472422]
29. Khuu A, Ren J, Dimitrov I, et al. Orientation of lipid strands in the extracellular compartment of muscle: effect on quantitation of intramyocellular lipids. Magn Reson Med. 2009; 61(1):16–21. [PubMed: 19097207]
30. Versluis MJ, Kan HE, van Buchem MA, Webb AG. Improved signal to noise in proton spectroscopy of the human calf muscle at 7 T using localized B1 calibration. Magn Reson Med. 2010; 63(1):207–211. [PubMed: 19918906]
31. Fissoune R, Janier M, Briguet A, Hiba B. In vivo assessment of mouse hindleg intramyocellular lipids by 1H-MR spectroscopy. Acad Radiol. 2009; 16(7):890–896. [PubMed: 19297209]
32. Fleckenstein JL, Canby RC, Parkey RW, Peshock RM. Acute effects of exercise on MR imaging of skeletal muscle in normal volunteers. AJR Am J Roentgenol. 1988; 151(2):231–237. [PubMed: 3260716]
33. Patten C, Meyer RA, Fleckenstein JL. T2 mapping of muscle. Semin Musculoskelet Radiol. 2003; 7(4):297–305. [PubMed: 14735428]
34. Damon BM, Gregory CD, Hall KL, Stark HJ, Gulani V, Dawson MJ. Intracellular acidification and volume increases explain R(2) decreases in exercising muscle. Magn Reson Med. 2002; 47(1):14–23. [PubMed: 11754438]
35. Saab G, Thompson RT, Marsh GD. Effects of exercise on muscle transverse relaxation determined by MR imaging and in vivo relaxometry. J Appl Physiol. 2000; 88(1):226–233. [PubMed: 10642385]
36. Ploutz-Snyder LL, Nyren S, Cooper TG, Potchen EJ, Meyer RA. Different effects of exercise and edema on T2 relaxation in skeletal muscle. Magn Reson Med. 1997; 37(5):676–682. [PubMed: 9126941]
37. Du J, Hamilton G, Takahashi A, Bydder M, Chung CB. Ultrashort echo time spectroscopic imaging (UTESI) of cortical bone. Magn Reson Med. 2007; 58(5):1001–1009. [PubMed: 17969110]
38. Techawiboonwong A, Song HK, Leonard MB, Wehrli FW. Cortical bone water: in vivo quantification with ultrashort echo-time MR imaging. Radiology. 2008; 248(3):824–833. [PubMed: 18632530]
39. Du J, Chiang AJT, Chung CB, et al. Orientational analysis of Achilles tendon and enthesis using an ultrashort echo time spectroscopic imaging sequence. Magn Reson Imaging. 2010; 28(2):178–184. [PubMed: 19695811]
40. Oatridge A, Herlihy AH, Thomas RW, et al. Magnetic resonance: magic angle imaging of the Achilles tendon. Lancet. 2001; 358(9293):1610–1611. [PubMed: 11716890]
41. Borthakur A, Mellon E, Niyogi S, Witschey W, Kneeland JB, Reddy R. Sodium and T1rho MRI for molecular and diagnostic imaging of articular cartilage. NMR Biomed. 2006; 19(7):781–821. [PubMed: 17075961]
42. Constantinides CD, Gillen JS, Boada FE, Pomper MG, Bottomley PA. Human skeletal muscle: sodium MR imaging and quantification-potential applications in exercise and disease. Radiology. 2000; 216(2):559–568. [PubMed: 10924586]

43. Bansal N, Szczepaniak L, Ternullo D, Fleckenstein JL, Malloy CR. Effect of exercise on (23)Na MRI and relaxation characteristics of the human calf muscle. J Magn Reson Imaging. 2000; 11(5): 532–538. [PubMed: 10813863]
44. Weber MA, Nielles-Vallespin S, Huttner HB, et al. Evaluation of patients with paramyotonia at 23Na MR imaging during cold-induced weakness. Radiology. 2006; 240(2):489–500. [PubMed: 16775221]
45. Nielles-Vallespin S, Weber MA, Bock M, et al. 3D radial projection technique with ultrashort echo times for sodium MRI: clinical applications in human brain and skeletal muscle. Magn Reson Med. 2007; 57(1):74–81. [PubMed: 17191248]
46. Park JH, Brown RL, Park CR, et al. Functional pools of oxidative and glycolytic fibers in human muscle observed by 31P magnetic resonance spectroscopy during exercise. Proc Natl Acad Sci U S A. 1987; 84:8976–8980. [PubMed: 3480522]
47. McCully KK, Boden BP, Tuchler M, Fountain MR, Chance B. Wrist flexor muscles of elite rowers measured with magnetic resonance spectroscopy. J Appl Physiol. 1989; 67(3):926–932. [PubMed: 2793723]
48. Minotti JR, Johnson EC, Hudson TL, et al. Training-induced skeletal muscle adaptations are independent of systemic adaptations. J Appl Physiol. 1990; 68(1):289–294. [PubMed: 2312472]
49. Yoshida T, Watari H. Metabolic consequences of repeated exercise in long distance runners. Eur J Appl Physiol Occup Physiol. 1993; 67:261–265. [PubMed: 8223541]
50. Ross BD, Radda GK, Gadian DG, Rocker G, Esiri M, Falconer-Smith J. Examination of a case of suspected McArdle's syndrome by 31P nuclear magnetic resonance. N Engl J Med. 1981; 304(22): 1338–1342. [PubMed: 6938778]
51. Gruetter R, Kaelin P, Boesch C, Martin E, Werner B. Non-invasive 31P magnetic resonance spectroscopy revealed McArdle disease in an asymptomatic child. Eur J Pediatr. 1990; 149(7): 483–486. [PubMed: 2347342]
52. de Kerviler E, Leroy-Willig A, Jehenson P, Duboc D, Eymard B, Syrota A. Exercise-induced muscle modifications: study of healthy subjects and patients with metabolic myopathies with MR imaging and P-31 spectroscopy. Radiology. 1991; 181(1):259–264. [PubMed: 1887044]
53. Zange J, Grehl T, Disselhorst-Klug C, et al. Breakdown of adenine nucleotide pool in fatiguing skeletal muscle in McArdle's disease: a noninvasive 31P-MRS and EMG study. Muscle Nerve. 2003; 27(6):728–736. [PubMed: 12766985]
54. Vorgerd M, Zange J. Carbohydrate oxidation disorders of skeletal muscle. Curr Opin Clin Nutr Metab Care. 2002; 5(6):611–617. [PubMed: 12394636]
55. Chance B, Eleff S, Bank W, Leigh JS Jr, Warnell R. 31P NMR studies of control of mitochondrial function in phosphofructokinase-deficient human skeletal muscle. Proc Natl Acad Sci U S A. 1982; 79(24):7714–7718. [PubMed: 6218501]
56. Edwards RHT, Dawson MJ, Wilkie DR, Gordon RE, Shaw D. Clinical use of nuclear magnetic resonance in the investigation of myopathy. Lancet. 1982; 1(8274):725–731. [PubMed: 6122019]
57. Vissing J, Vissing SF, MacLean DA, Saltin B, Quistorff B, Haller RG. Sympathetic activation in exercise is not dependent on muscle acidosis. Direct evidence from studies in metabolic myopathies. J Clin Invest. 1998; 101(8):1654–1660. [PubMed: 9541495]
58. Taivassalo T, De Stefano N, Argov Z, et al. Effects of aerobic training in patients with mitochondrial myopathies. Neurology. 1998; 50(4):1055–1060. [PubMed: 9566394]
59. Kuhl CK, Layer G, Träber F, Zierz S, Block W, Reiser M. Mitochondrial encephalomyopathy: correlation of P-31 exercise MR spectroscopy with clinical findings. Radiology. 1994; 192(1): 223–230. [PubMed: 8208943]
60. Schunk K, Romaneehsen B, Rieker O, et al. Dynamic phosphorus-31 magnetic resonance spectroscopy in arterial occlusive disease: effects of vascular therapy on spectroscopic results. Invest Radiol. 1998; 33(6):329–335. [PubMed: 9647444]
61. Kemp GJ, Hands LJ, Ramaswami G, et al. Calf muscle mitochondrial and glycogenolytic ATP synthesis in patients with claudication due to peripheral vascular disease analysed using 31P magnetic resonance spectroscopy. Clin Sci (Lond). 1995; 89(6):581–590. [PubMed: 8549076]

62. Scheuermann-Freestone M, Madsen PL, Manners D, et al. Abnormal cardiac and skeletal muscle energy metabolism in patients with type 2 diabetes. Circulation. 2003; 107(24):3040–3046. [PubMed: 12810608]

63. Petersen KF, Befroy D, Dufour S, et al. Mitochondrial dysfunction in the elderly: possible role in insulin resistance. Science. 2003; 300(5622):1140–1142. [PubMed: 12750520]

64. Kent-Braun JA, Ng AV, Doyle JW, Towse TF. Human skeletal muscle responses vary with age and gender during fatigue due to incremental isometric exercise. J Appl Physiol. 2002; 93(5): 1813–1823. [PubMed: 12381770]

65. Horská A, Fishbein KW, Fleg JL, Spencer RG. The relationship between creatine kinase kinetics and exercise intensity in human forearm is unchanged by age. Am J Physiol Endocrinol Metab. 2000; 279(2):E333–E339. [PubMed: 10913033]

66. Bogner W, Chmelik M, Schmid AI, Moser E, Trattnig S, Gruber S. Assessment of (31)P relaxation times in the human calf muscle: a comparison between 3 T and 7 T in vivo. Magn Reson Med. 2009; 62(3):574–582. [PubMed: 19526487]

67. Duong TQ, Yacoub E, Adriany G, et al. High-resolution, spin-echo BOLD, and CBF fMRI at 4 and 7 T. Magn Reson Med. 2002; 48(4):589–593. [PubMed: 12353274]

68. Yacoub E, Van De Moortele PF, Shmuel A, Uğurbil K. Signal and noise characteristics of Hahn SE and GE BOLD fMRI at 7 T in humans. Neuroimage. 2005; 24(3):738–750. [PubMed: 15652309]

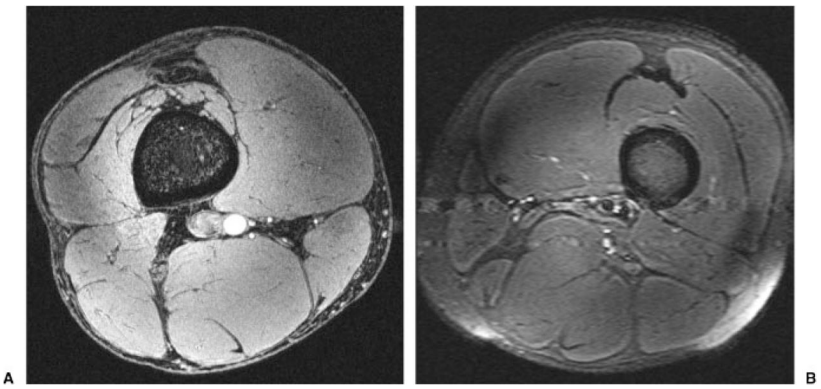

Figure 1.

(A) Axial T1-weighted 7-T magnetic resonance (MR) image of the thigh from a healthy male volunteer (3D gradient-recalled echo; TR/TE, 20 ms/4 ms; field of view [FOV], 13 cm × 13 cm; matrix, 512 × 512, 0.253 mm × 0.253 mm; slice thickness, 1 mm). Incidental note is made of flow-related enhancement within the popliteal artery. (B) Axial T2-weighted 7-T MR image of the thigh from a healthy male volunteer (turbo spin-echo; TR/TE, 3000 ms/60 ms; FOV, 16 cm × 16 cm; matrix, 256 × 256, 0.625 mm × 0.625 mm; slice thickness, 2 mm) in a different subject. There is pulsation artifact and coil inhomogeneity artifact near the periphery of the FOV.

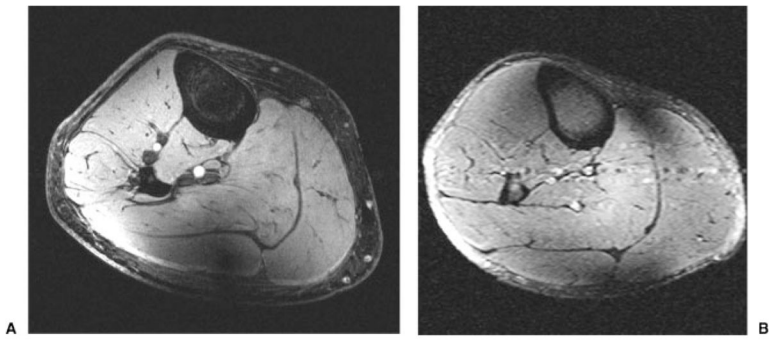

Figure 2.

(A) Axial T1-weighted 7-T magnetic resonance (MR) image of the calf from a healthy female volunteer (3D gradient-recalled echo; TR/TE, 20 ms/4 ms; field of view [FOV], 15 cm; matrix, 512 × 512, 0.292 mm × 0.292 mm; slice thickness, 2 mm). Incidental note is made of flow-related enhancement within the arteries and coil inhomogeneity artifact posteriorly. (B) Axial T2-weighted 7-T MR image of the calf from a healthy male volunteer (turbo spin-echo; TR/TE, 3000 ms/60 ms; FOV, 15 cm × 15 cm; matrix, 256 × 256, 0.585 mm × 0.585 mm; slice thickness, 2 mm). There is pulsation artifact and coil inhomogeneity artifact near the periphery of the FOV.

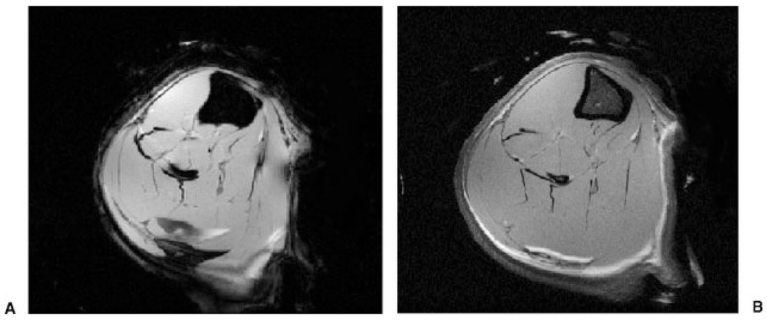

Figure 3.

(A) High-resolution axial 11.7-T magnetic resonance (MR) image of the tibia and fibula of a male Sprague-Dawley rat obtained ex vivo (gradient echo; TR/TE, 500 ms/5.07 ms; signal averages, 4; field of view [FOV], 1.7 cm × 1.7 cm; matrix, 256 × 256, 0.066 mm × 0.066 mm; slice thickness, 0.5 mm). Chemical shift artifact at fat-muscle interfaces can be appreciated. (B) High-resolution axial 11.7-T MR image of the tibia and fibula of a male Sprague-Dawley rat obtained ex vivo (spin echo; TR/TE, 2500 ms/8.0 ms; signal averages, 2; FOV, 1.6 cm × 1.6 cm; matrix, 512 × 512, 0.031 mm × 0.031 mm; slice thickness, 0.5 mm). The difference in contrast between bone marrow, muscle, and fat at 11.7 T can be appreciated.

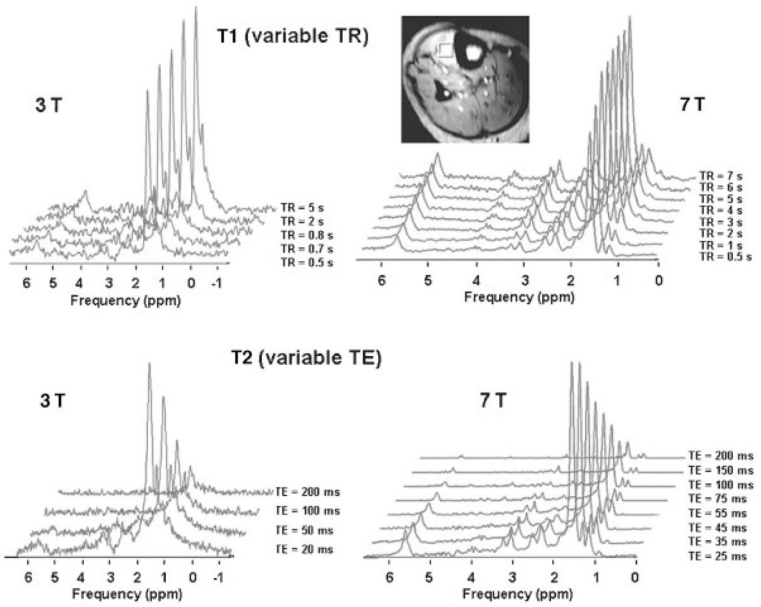

Figure 4.

Representative stacked T_{11}(variable TR) and T2 (variable TE) spectra of metabolites from the tibialis anterior muscle of a healthy male volunteer using the stimulated echo acquisition mode (STEAM) pulse sequence at 3 T and 7 T. A voxel of 10 mm × 10 mm × 10 mm was positioned and used for localized proton spectra (7-T localizer image shown). Image from Wang et al.[28]

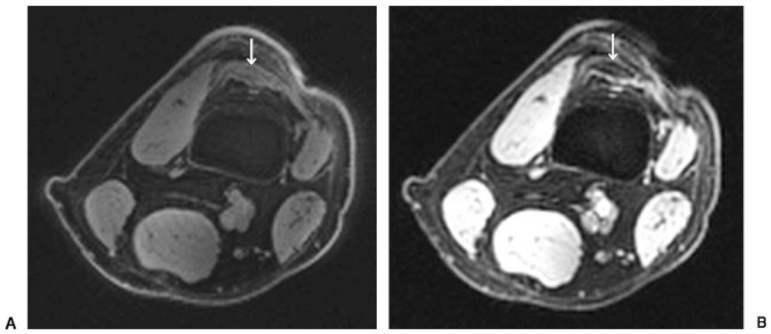

Figure 5.

(A) Axial ultra-short echo-time image of the distal thigh from a healthy male volunteer (TR/TE, 250 ms/0.300 ms; 3D radial acquisition; 25,000 projections, 1.48 × 1.48 × 1.48 mm) demonstrates uniform hyperintense signal within the quadriceps tendon (arrow). Incidental note is made of minimal signal within cortical bone of the femur. (B) Axial image of the distal thigh from a healthy male volunteer (obtained at the same level and with the same parameters as in Fig. 3A with the exception of TE, 4.4 ms) demonstrates only minimal signal within the quadriceps tendon centrally (arrow).

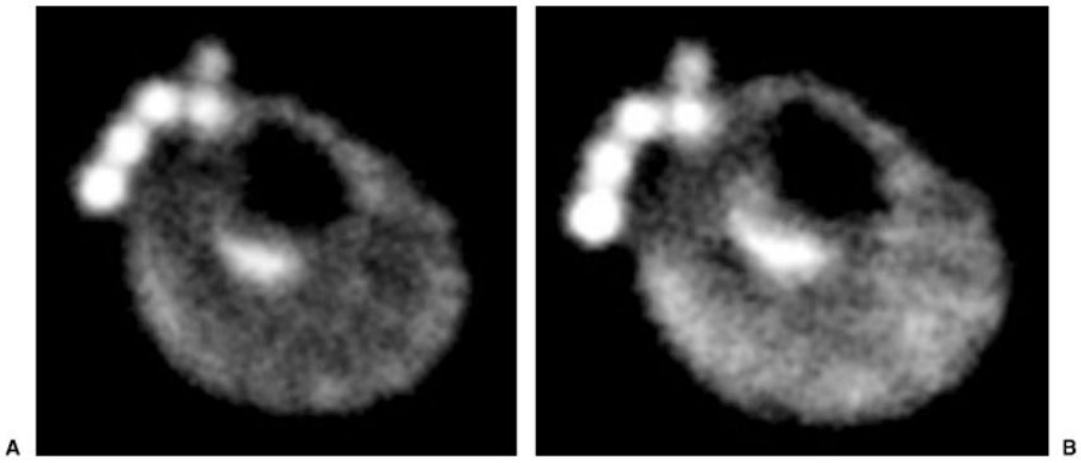

Figure 6.

(A) Resting axial ^{23}Na 7-T magnetic resonance (MR) image from a healthy male volunteer demonstrates uniform signal intensity in the muscles of the calf. At the anterior aspect of the leg, phantoms containing NaCl of different concentrations (100 mmol, 150 mmol, 200 mmol, 250 mmol, and 300 mmol) are seen. (B) After 3 minutes of plantar flexion exercise, ^{23}Na 7-T MR image demonstrates increased signal intensity within the posterior compartment muscles of the calf (gastrocnemius and soleus) used in the exercise. At the anterior aspect of the leg, phantoms containing NaCl of different concentrations (100 mmol, 150 mmol, 200 mmol, 250 mmol, and 300 mmol) are seen.

Table 1

Comparison of T1 and T2 Relaxation Times for Skeletal Muscle Metabolites at 3 T and 7 T

Comparison of T_1 Relaxation Times in Tibialis Muscle (TA) at 3 T and 7 T									
TA	**IMCL-CH_3 (0.9 ppm)**	**EMCL-CH_3 (1.1 ppm)**	**IMCL-CH_2 (1.27 ppm)**	**EMCL-CH_2 (1.5 ppm)**	**= =CH-CH_2-$(CH_2)_n$ (2.24 ppm)**	**-CO-CH_2-CH= = (2.4 ppm)**	**Cr-CH_3 (3.03 ppm)**	**TMA (3.2ppm)**	**-CH= =CH- (5.4 ppm)**
3 T (ms)	866 ± 216	440 ± 108	546 ± 115	372 ± 119	NM*	NM	900 ± 147	1095 ± 268	NM
7 T (ms)	1946 ± 606	1427 ± 338	1494 ± 158	2187 ± 1001	1372 ± 239	1971 ± 235	1632 ± 164	1339 ± 40	2036 ± 404
Change (%)	125	224	174	488	NM	NM	81	22	NM
Comparison of T_2 Relaxation Times in Tibialis Muscle (TA) at 3 T and 7 T									
TA	**IMCL-CH_3 (0.9 ppm)**	**EMCL-CH_3 (1.1 ppm)**	**IMCL-CH_2 (1.27ppm)**	**EMCL-CH_2 (1.5 ppm)**	**= =CH-CH_2-$(CH_2)_n$ (2.24 ppm)**	**-CO-CH_2-CH= = (2.4 ppm)**	**Cr-CH_3 (3.03 ppm)**	**TMA (3.2 ppm)**	**-CH= =CH- (5.4 ppm)**
3 T (ms)	68 ± 6	64 ± 16	75 ± 5	81 ± 3	NM	NM	131 ± 14	110 ± 19	NM
7 T (ms)	42 ± 12	53 ± 1	56 ± 4	64 ± 7	28 ± 7	29 ± 8	53 ± 6	39 ± 3	56 ± 21
Change (%)	38	17	25	21	NM	NM	60	65	NM

The peaks at 2.24 ppm, 2.4 ppm, and 5.4 ppm were not measurable (NM) at 3 T but could be resolved and measured at 7 T. At 7 T, T1 values increase and T2 values decrease compared with 3 T.

IMCL, intramyocellular lipid; EMCL, extramyocellular lipid; NM, not measurable.

From Wang et al.[28]